Journal of Electroanalytical Chemistry 794 (2017) 189–196

Contents lists available at ScienceDirect

Journal of Electroanalytical Chemistry

journal homepage: www.elsevier.com/locate/jelechem

On the electrocatalytic urea oxidation on nickel oxide nanoparticles modified glassy carbon electrode

Reham H. Tammam[a,*], Mahmoud M. Saleh[a,b,*]

[a] Department of Chemistry, Faculty of Science, Cairo University, Cairo, Egypt
[b] Chemistry Department, College of Science, King Faisal University, Al-Hassa, Kingdom of Saudi Arabia

ARTICLE INFO

Keywords:
Urea
Oxidation
Nanoparticles
Electrocatalysis
Nickel

ABSTRACT

Electrochemical impedance spectroscopy (EIS) and cyclic voltammetry (CV) are used here to investigate the electrochemical characteristics of the urea oxidation on nickel oxide (NiO_x) nanoparticles modified glassy carbon (GC) electrode from alkaline 0.5 M NaOH solution. The effects of NiO_x loading and urea concentration on urea electrocatalytic oxidation are discussed in the light of the EIS data and corresponding equivalent circuits. The Nyquist plots show semicircles with fitting parameters that are dependent on the applied conditions. Charge transfer resistance is found to be lower in presence of urea due to higher rates of urea electrooxidation. Cyclic voltammetry (CV) helps to investigate the catalytic properties of urea oxidation on the GC/NiO_x. The relation between the peak current of urea oxidation and the potential scan rate are measured and fitted with that calculated by Randles-Sevcik equation. The results indicate a diffusion-controlled irreversible process. Optimization of the loading extent of NiO_x and interpretation of the effect of urea concentration is enabled from the CVs, EIS and equivalent circuit parameters.

1. Introduction

Energy demand, environmental pollution and clean waters have been considered as closely interlinked and overlapped research areas that gained a continuous and growing attention. While the search for new energy sources continues to be a milestone, the prevention of water pollution, on the other hand, is a challenge for scientists and engineers worldwide. Water treatment and remediation are considered to be crucial for clean and safe water resources. An interesting conversion that may include the above three elements of the triangle is the electrocatalytic oxidation of urea. Electrocatalytic oxidation of urea has gained a growing attention during the last decades. While some workers considered urea as an organic waste and should be removed before its disposal to the environment [1,2], some authors considered it as fuel in what is so called direct urea fuel cell [3–5]. Others, on the other hand, studied the possibility of producing hydrogen gas as an interesting product from urea electrooxidation [6–10].

Hydrogen production via processing of the abundantly available wastewaters has been gaining more consideration during the last decade [11–13]. Studies have been reported in using industrial waters of high concentrations of urea for the synthesis of H_2 gas in basic solutions [14,15]. Municipal waters, on the other hand, contain relatively high concentrations of urea as for accumulated human and animal urines [14,15]. Urea is produced in many industries with large percentages and this finds its ways to the environment via ground waters with relatively high concentrations of urea and its derivatives. Biodegradation of those molecules to NO_2^- and NO_3^- may result in many diseases to human [16].

In this context, denitrification method is not that cheap and has low capacity and hence better techniques should be developed. Electrolysis of urea solution (in NaOH for example) can be considered as an anodic urea oxidation producing nitrogen and carbon dioxide and H_2 gas at the cathode. The latter with high purity can be considered as a desirable fuel with high purity by-product [17]. In combination with waste water treatment units, the latter electrolysis process can be considered as an economically feasible process when compared with other techniques [17].

It has long been known that Pt-based electrocatalysts are the unavoidable candidate for oxidation of organic molecules. However, Ni-based electrocatalysts can represent good substituent for the above electrocatalysts especially for small molecules [18–21]. Some authors [22,23] demonstrated the anodic oxidation of urea from alkaline solutions at Ni-based electrocatalysts. Urea electrooxidation at nickel oxide in an alkaline medium can take place according to the following reactions [23]:

Anode:

* Corresponding authors.
E-mail addresses: reham_tammam@cu.edu.eg (R.H. Tammam), mmsaleh@kfu.edu.sa, mahmoudsaleh90@yahoo.com (M.M. Saleh).

http://dx.doi.org/10.1016/j.jelechem.2017.04.023
Received 21 January 2017; Received in revised form 15 April 2017; Accepted 17 April 2017
Available online 19 April 2017

$$Ni(OH)_{2(s)} + OH^- \rightleftarrows NiOOH_{(s)} + H_2O_{(l)} + e^- \quad (1)$$

$$CO(NH_2)_{2(aq)} + 6OH^- \rightarrow N_{2(g)} + 5H_2O_{(l)} + CO_{2(g)} + 6e^- \quad (2)$$

Cathode:

$$6H_2O_{(l)} + 6e^- \rightarrow 3H_{2(g)} + 6OH^- \quad (3)$$

Overall:

$$CO(NH_2)_{2(aq)} + H_2O_{(l)} \rightarrow N_{2(g)} + 3H_{2(g)} + CO_2(g) \quad (4)$$

In the above electrochemical steps, it is believed that Ni (II) is oxidized to Ni (III) (see Eq. (1)) and the latter poses its role in the anodic oxidation of urea. Different important electrocatalytic reactions such as methanol and glucose oxidation on transition metal oxides were studied using EIS techniques [24,25]. A better understanding of urea electrooxidation on Ni-oxides can be achieved using this technique. In the other hand, enzymeless sensors for detection of urea using metal and metal oxide nanoparticles modified electrodes have been reported [26,27].

Despite a large number of articles dealing with electrochemical oxidation of urea on Ni and NiO-based electrocatalysts, few number of those articles used Ni-based electrocatalysts synthesized via electrochemical routes. Synthesis methods for Ni and NiO- based catalysts include (but not limited to) hydrothermal process [13,28,29], chemical deposition [30], impregnation method [31] and reflux-based method [32]. In other article, Ni-foam has been used [33]. While some authors electrochemically prepared Ni-based catalysts in nano size [34,35], others synthesized Ni-based catalysts as bulk materials [22,36]. Clearly, using Ni electrocatalysts in nanosize have many advantages. We will see in the "Results and discussion" section that our electrode (GC/NiO_x) synthesized in nanosize is superior to that synthesized in bulky size. Also, urea electrochemical oxidation either studied by cyclic voltammetry measurements [37] or EIS measurements [34]. Finding an article using both techniques is considered to be scarce [38]. In our work here, both techniques have been used. This may help to better understanding of the process.

The purpose of the present work is to gain a more insight into the characterization of the electrocatalytic oxidation of urea on NiO_x nanoparticles modified GC electrode in alkaline medium. Different electrochemical techniques such as electrochemical impedance spectroscopy (EIS) and cyclic voltammetry (CV) are going to be used to discuss the electrochemical characteristic parameters of the electrocatalytic oxidation of urea from alkaline NaOH solutions. Surface characterization is done by scanning electron microscopy (SEM).

2. Experimental

2.1. Measurements

All the reagents used in this work were Merck and Sigma-Aldrich products of analytical grade and were used without further purification. The working electrode was GC (d = 3.0 mm). It was cleaned by mechanical polishing with aqueous slurries of successively finer alumina powder (down to 0.06 mm) then washed thoroughly with water. An $Hg/Hg_2Cl_2/KCl$ (sat) (SCE) and a Pt sheet were used as a reference and counter electrodes, respectively. An electrochemical cell with a three-electrode configuration was used in this study at 25 °C. Electrochemical characterizations were performed using system IM6 Zahner electrik Meβtechnik, Germany. The experimental impedance spectra were fitted with the appropriate equivalent circuits using the "SIM" program included with the IM6 package. The suitability of the elements in the proposed equivalent circuits to fit the experimental data was judged by the error% of the fitting and by comparing the calculated and the experimental impedance plots. The frequency range of 100 kHz to 100 mHz and the modulation amplitude of 10 mV were employed for impedance measurements. Images of the scanning electron microscope (SEM) were taken using field emission scanning electron microscope, FE-SEM (FEI, QUANTA FEG 250).

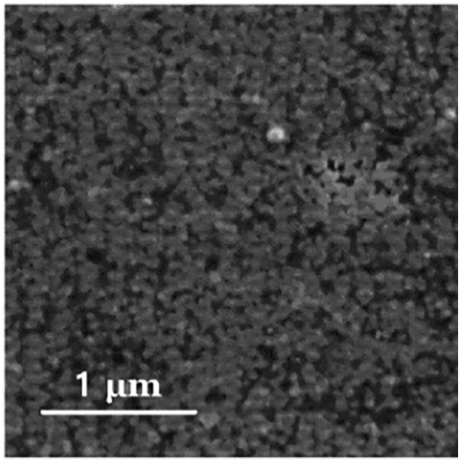

Fig. 1. SEM image of GC/NiO_x.

2.2. Electrode preparation

Details on modification procedure can be found elsewhere [39,40]. For instance, potentiostatic deposition of metallic nickel on the working electrode (i.e., GC) from an aqueous solution of 0.1 M acetate buffer solution (ABS, pH = 4.0) containing 1 mM $Ni(NO_3)_2{\cdot}6H_2O$ by applying a constant potential electrolysis of − 1 V for different time durations. Then, passivation of the metallic Ni in 0.1 M phosphate buffer solution (PBS, pH = 7) by cycling the potential between − 0.5 and 1 V for 20 cycles at a scan rate of 200 mV s^{-1}. The loading level of the nickel was estimated using chemical analysis by dissolution of the electrodeposited nickel with HNO_3 and then using a Perkin–Elmer 2380 atomic absorption spectrometer for the measurement.

3. Results and discussion

3.1. Characterization of GC/NiO_x

Fig. 1 presents a SEM micro image of NiO_x nanoparticles electrodeposited on GC electrode (for the duration of 10 min). The image demonstrates nanoparticles of NiO_x with considerable uniform distribution and the average size of 90 nm (± 10 nm). It is noteworthy to mention that potentiostatic deposition of metallic nickel is the first target in our electrodeposition procedure. Note that there is a possibility of forming nickel hydroxide during the electrodeposition of nickel [41]. To convert nickel to nickel oxide, a passivation procedure was carried out as described in the experimental section. The first, fifth and the tenth cycles of ten successive potential scans of the passivation process in PBS (pH = 7) are shown in Fig. 2. An oxidation wave was observed at the first CV corresponding to the active anodic dissolution and passivation of the electrodeposited metallic nickel with a concurrent transformation between the different phases of nickel oxides. The following successive nine CVs support negligible anodic currents, indicating that a complete passivation of the surface layers of Ni has been achieved during the first CV cycle. Interestingly, the absence of any significant reduction peak in the cathodic scan, within the studied potential range, indicates that the passive nickel oxide nanoparticles are stable within the employed potential range and operating pH [40].

Fig. 3 shows CV responses for GC/NiO_x at different loadings of NiO_x in 0.5 M NaOH at a scan rate of 100 mV s^{-1}. The loading of NiO_x was controlled by controlling the time period of electrodeposition. The time periods used here in this work are 2, 4, 10, 20 and 40 min. In order to estimate the loading level of nickel during electrodeposition, chemical analysis process has been used as given in the Experimental section. The estimated values of the NiO_x loading levels are; 0.043, 0.087, 0.169,

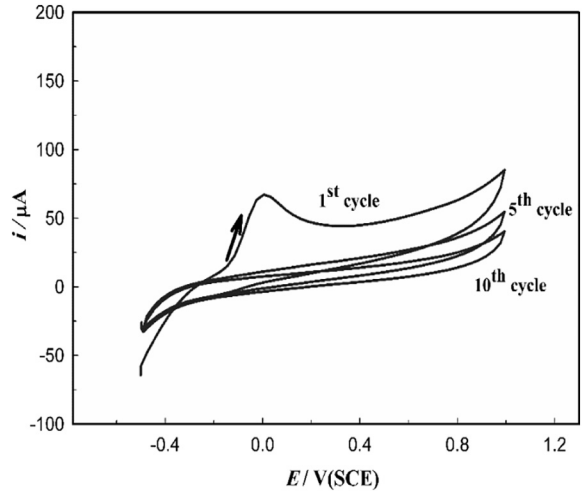

Fig. 2. CVs represent the first, seventh and tenth cycles of 10 successive potential cycles obtained at Ni/GC in 0.1 M PBS (pH = 7) at a scan rate of 200 mV s^{-1}.

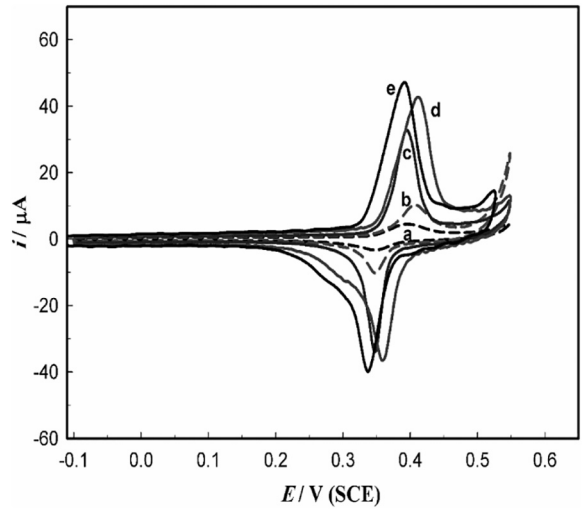

Fig. 3. CV responses for GC/NiO_x at different loadings of NiO_x in 0.5 M NaOH at scan rate 100 mV s^{-1}. The loadings are: (a) 0.04, (b) 0.091, (c) 0.173, (d) 0.465 and (e) 1.02 mg cm^{-2}.

0.435and 0.976 mg cm^{-2}. Also, the loading level of nickel was estimated from the charge passed during the electrodeposition process as follows. Transient current-time relations (*i-t*) were reordered at different conditions both in Ni^{2+}-free solution (gives i_H) and in a solution containing Ni^{2+} ions (gives total current, i_t). Subtracting the total current ($i_t = i_{Ni} + i_H$) from the current passed in blank solution (Ni^{2+} ion-free solution) i_H gives the current of nickel electrodeposition, i_{Ni}. From the above currents, the charge for Ni electrodeposition, Q_{Ni} was estimated. The latter values enabled us to estimate the loading levels of nickel using Faraday's law. The estimated values of the NiO_x loading levels are: 0.04, 0.091, 0.173, 0.465 and 1.02 mg cm^{-2}. Table 1A lists such values at the different time periods of electrodeposition. Note that the values of the loading level determined from chemical analysis and from Q_{Ni} are comparable. Table 1A also lists the values of the charge passed during the passivation process, Q_{pas} as estimated from Fig. 2 and lists the passivation index, α ($\alpha = Q_{pas}/Q_{Ni}$). The values of α are much less than one and decrease with the loading extent. It indicates that not all the Ni layers are converted to the oxide and more difficult diffusion into the solid matrix prevents further conversion.

A known strategy for activation of the GC/NiO_x electrode was followed in the present work. This was done by cycling the potential in the range of 0.1 to 0.6 V in 0.5 M NaOH solution. During the potential cycling, the current increases (CVs are not shown here) up to 20 cycles after which no further increase of the peak current was observed. Thus, the CV of GC/NiO_x at each loading as given in Fig. 3 is the recorded CV after the consecutive 20 cycles. As the loading extent increases, the peak current of the anodic sweep of the $Ni(OH)_2$/NiOOH increases. There is also a negative shift in the onset potential of the $Ni(OH)_2$/NiOOH redox couple. The increase of the peak current with the extent of loading may be attributed to the progressive enrichment of the accessible electroactive species, $Ni(OH)_2$ and NiOOH on the electrode surface. The surface concentration, Γ of the nickel hydroxide species can be estimated from the charge (Q_{tran}) consumed during the redox transformation of Ni(II)/Ni(III) from the CVs in Fig. 3 (i.e., $\Gamma = Q_{tran}/nF$). The values of Γ and the index of activation, β are listed in Table 1B. The β value is the ratio of Q_{tran}/Q_{Ni}. It is obvious that the values of β are much lower than one and decreases with the Ni loading. This point to the fact that not all the Ni layers are converted to the oxide (see the passivation index, α in Table 1A) and not all the oxide layers are converted to hydroxide (see the activation index, β in Table 1B). Using the crystallographic value for a $Ni(OH)_2$ monolayer of 1.06×10^{-9} mol cm^{-2}as obtained from Bode et al. and others [41,42] and considering the values of Γ, the number of surface monolayers at the different Ni loadings are: 6.5, 12.9, 26.5, 46.1 and 52.4 at time periods of 2, 4, 10, 20 and 40 min, respectively.

Fig. 4 shows a Nyquist diagram for GC/NiO_x at different loadings of NiO_x in 0.5 M NaOH at $E = 0.375$ V. The figure reveals depressed semicircle with a diameter dependent on the loading extent. Fitting of the above EIS data was done using the equivalent circuit shown in the

Table 1B
Values of the charge of the Ni(II)/Ni(III) transform at different time durations, the number of $Ni(OH)_2$ monolayer and the activation index, β.

t/min	Q_{tran}/mC	Γ/mmol $cm^{-2} \times 10^{-6}$	Number of Ni $(OH)_2$ monolayer	$\beta = Q_{tran}/Q_{Ni} \times 10^{-3}$
2	0.047	6.9	6.5	4.96
4	0.093	13.7	12.9	4.42
10	0.191	28.1	26.5	4.76
20	0.330	48.8	46.1	3.08
40	0.375	55.5	52.4	1.60

Table 1A
Values of the charge consumed in the nickel deposition and hydrogen evolution reaction at GC electrode at different time durations. The table also shows the charge consumed during the passivation process and the index of passivation, α.

t/min	Loading/mg cm^{-2} from Chem. Anal	Q_{Ni+H2}/mC	Q_{H2}/mC	Q_{Ni}/mC	Loading/mg cm^{-2} from Q_{Ni}	Q_{Pas}/mC	$\alpha = Q_{pas}/Q_{Ni} \times 10^{-3}$
2	0.043	10.36	1.96	9.40	0.04	0.163	17.9
4	0.087	24.54	3.53	21.01	0.091	0.183	9.0
10	0.169	48.08	8.16	39.92	0.173	0.427	11.0
20	0.435	122.89	15.72	107.16	0.465	1.03	9.6
40	0.976	292.86	28.10	234.76	1.02	1.84	8.0

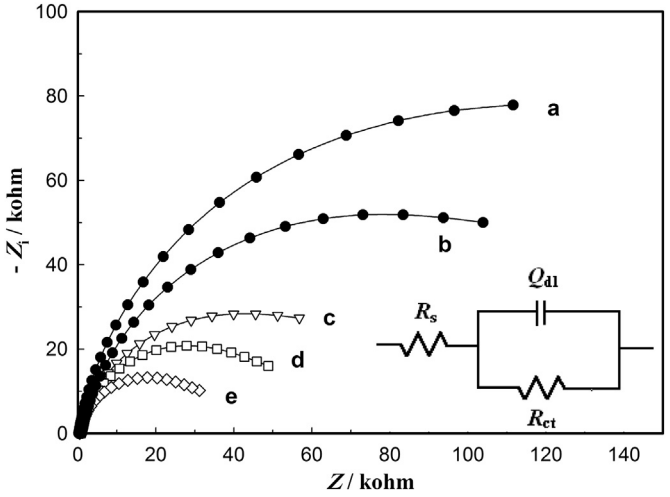

Fig. 4. Nyquist diagrams for GC/NiO_x electrode at different loadings of NiO_x in 0.5 M NaOH(blank) at E = 0.375 V. The loadings are: (a) 0.04, (b) 0.091, (c) 0.173, (d) 0.465 and (e) 1.02 mg cm^{-2}.The inset shows the equivalent circuit that represents Nyquist diagram in Fig. 4.

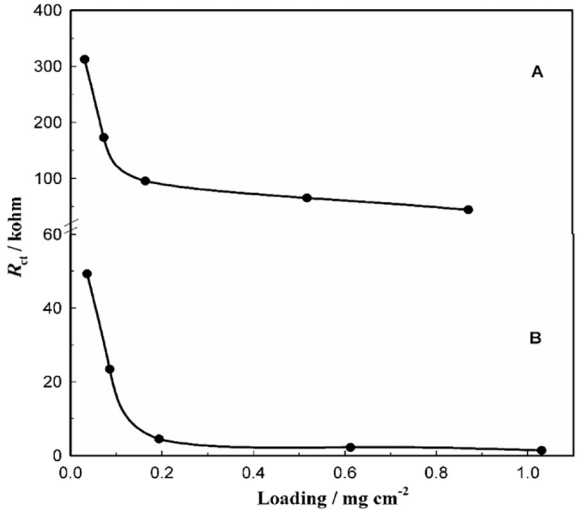

Fig. 5. Change of the R_{ct} values with the loading extent of NiO_x in (A) blank 0.5 M NaOH and (B) in 0.5 M NaOH containing 0.2 M urea.

inset of Fig. 4 and the fitting parameters are listed in Table 2. These are: the solution resistance, R_s, the charge transfer resistance, R_{ct} and constant phase element, *CPE* (Q_{dl} in the inset of Fig. 4). One can say that GC/NiO_x follows Randels equivalent circuit except that the capacitor of the double layer (C_{dl}) deviated from a pure capacitor due to inhomogeneity and surface roughness of the electrode and thus it is replaced by *CPE* as shown in the equivalent circuit in Fig. 4. Note that the symbol *n* in Table 2 is defined as an empirical value that accounts for the deviation from the ideal capacitive behavior due to surface inhomogeneity and roughness [25]. The *n* values as shown in Table 2 are less than one indicating a roughness of the NiO_x surface as for an electrodeposited of NiO_x nanoparticles on the GC electrode.

As revealed from Table 2, as the loading extent increases, the R_{ct} decreases pointing to the faster charge transfer of the redox couple (Ni$(OH)_2$/NiOOH). This can be attributed to the increase in the concentration of the active species $Ni(OH)_2$ and NiOOH with the increase of the loading extent. The results in Fig. 4 are in accordance with the CVs obtained in Fig. 3. The change of R_{ct} with the loading extent for the blank solution can be seen in Fig. 5 (curve A). There is an initial fast decrease in the R_{ct} followed by slow decrease after loading > 0.173 mg cm^{-2} (t_{dep} > 10 min). This slower decrease in R_{ct} (i.e., a slower increase of charge transfer rate) was attributed to increased generation of inactive β-$Ni(OH)_2$ and slow diffusion of the hydroxide ions into the limited wettable electrode surface [43]. A tradeoff between the increased loading of the $Ni(OH)_2$ and the possible slow conversion of a fraction of the α-$Ni(OH)_2$ species to β-$Ni(OH)_2$ which is evident also from literature [44,45].

Table 2
Equivalent circuit parameters of GC/NiO_x electrode in 0.5 M NaOH solution (blank) obtained from Fig. 4 at different time loading of Ni at E = 0.375 V.

Time/min	R_s/Ω	R_{ct}/kΩ	Q_{dl}/μF	*n*
2	28.1	312.6	3.73	0.87
4	28.1	173.0	10.34	0.89
10	28.5	95.6	22.32	0.88
20	30.3	65.2	28.47	0.89
40	30.2	44.1	31.48	0.89

3.2. Electrocatalytic oxidation of urea

Fig. 6 shows CV responses of GC/NiO_x (loading = 0.173 mg cm^{-2}) in 0.5 M NaOH (A) and in 0.5 M NaOH containing 0.2 M urea (B) at scan rate 20 mV s^{-1}. The CV in the blank (urea-free electrolyte) (curve A) shows a pair of redox peaks at ~0.4 V and ~0.35 V in the anodic and cathodic sweep, respectively. This pair corresponds to the Ni$(OH)_2$ ↔ NiOOH redox couple. In presence of 0.2 M urea (curve B) high anodic current peak at E ~ 0.47 V is observed in the forward scan which points to an enhancement of the electrochemical oxidation of urea on the GC/NiO_x electrode. In the backwards scan, another peak at ~0.45 V is observed. This peak lies in the range of urea oxidation and may be attributed to the further electrochemical urea oxidation on the regenerated active surface sites (Ni(II)/Ni(III)) [46]. Note that the anodic peak in the reverse scan is lower than that of the forward scan due to the incomplete regeneration of the active sites on the electrode surface. Electrocatalytic mechanism is evident since the cathodic peak for the Ni(III) → Ni(II) conversion decreases significantly in presence of urea [46]. It is noteworthy to mention that from the thermodynamic point of view, the oxygen evolution reaction, OER can be considered as a side reaction. However, OER is kinetically controlled reaction

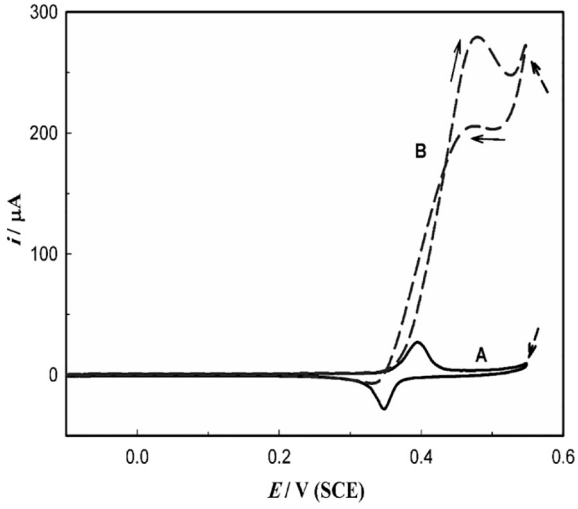

Fig. 6. CV responses for GC/NiO_x (loading = 0.173 mg cm^{-2}) in 0.5 M NaOH in absence (A) and in presence (B) of 0.2 M urea using scan rate of 20 mV s^{-1}.

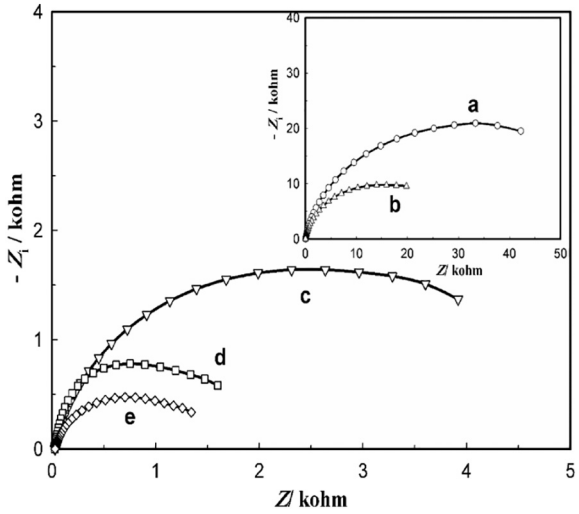

Fig. 7. Nyquist diagrams for GC/NiO_x electrode at different loadings of NiO_x in 0.5 M NaOH containing 0.2 M urea at E = 0.4 V. The loadings are: (a) 0.04, (b) 0.091, (c) 0.173, (d) 0.465 and (e) 1.02 mg cm^{-2}.

Table 3
Equivalent circuit parameters for electrooxidation of urea from 0.5 M NaOH containing 0.2 M urea on GC/NiO_x electrode at different time of loadings obtained from Fig. 6 at E = 0.4 V.

Time/min	R_s/Ω	R_{ct}/kΩ	Q_{dl}/μF	n
2	30.6	49.3	4.85	0.87
4	30.9	23.4	10.73	0.88
10	29.3	5.1	23.40	0.86
20	31.1	2.5	30.50	0.86
40	31.9	1.4	37.13	0.83

especially on metal oxide modified electrodes [47]. From Fig. 6, we can find that the onset potential of the OER (see dashed arrows in Fig. 6) is ~0.55 V (SCE) and yet it does not interfere with the urea electrooxidation. However, subtraction of the CV (in presence of urea) from the background current (urea-free electrolyte) is done as shown in Figs. 8 and 9 (*c.f.*, the following section).

Fig. 7 shows a Nyquist plot of GC/NiO_x with different loading extents of NiO_x nanoparticles in 0.5 M NaOH containing 0.2 M urea at E = 0.4 V. The Nyquist plot reveals depressed semicircle with a diameter decreasing with the loading extent of NiO_x. The EIS data in Fig. 7 was fitted with the equivalent circuit shown in the inset of Fig. 4 and the resulting fitting parameters are listed in Table 3. The charge transfer resistance of the electrochemical oxidation of urea at the GC/NiO_x electrode has the physical significance of: how facile and what is the rate of the charge transfer during the electrocatalytic oxidation of urea and what are the effects of the different variables such as the loading extent on its value.

Comparing the values of R_{ct} in Tables 2 and 3 indicates that the presence of urea increases the rate of charge transfer (as R_{ct} (urea) < R_{ct} (blank)). This may be attributed to the higher rates of electrocatalytic oxidation of urea on the GC/NiO_x. The change of R_{ct} with the loading extent is shown in Fig. 5B. As the loading extent increases, the R_{ct} decreases dramatically at first before it slowly decreases. At loading > 0.173 mg cm^{-2} (t_{dep} > 10 min) insignificant change of the R_{ct} is observed. We can say that t_{dep} of 10 min is optimum for urea oxidation at the present experimental conditions. It is note of worthy to mention that the values of R_s (solution resistance) are in general slightly higher in presence of urea. This may be attributed to the conversion of the OH^- ions (high conductivity) to CO_3^{2-} ions due to the following reaction of the produced CO_2; $CO_2 + OH^- \rightarrow CO_3^{2-}$.

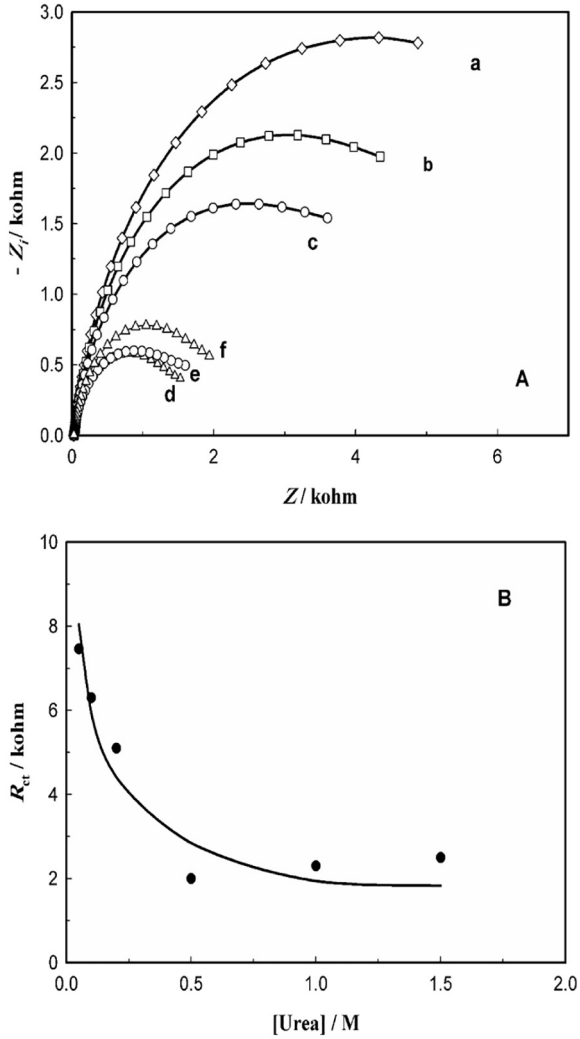

Fig. 8. (A) Nyquist diagrams for GC/NiO_x electrode at loading of NiO_x = 0.173 mg cm^{-2}in 0.5 M NaOH containing different concentrations of urea at E = 0.4 V. The concentrations are: (a) 0.05, (b) 0.1, (c) 0.2, (d) 0.5 (e) 1.0 M and (f) 1.5 M. (B) change of R_{ct} with [urea].

Table 4
Equivalent circuit parameters for electrooxidation of urea on GC/NiO_x electrode in 0.5 M NaOH containing different concentrations of urea obtained from Fig. 7A at E = 0.4 V.

[urea]/M	R_s/Ω	R_{ct}/kΩ	Q_{dl}/μF	n
0.05	29.7	7.46	16.91	0.84
0.1	30.9	6.3	18.39	0.84
0.2	29.3	5.1	23.4	0.86
0.5	30.9	2.0	24.0	0.86
1	31.8	2.3	23.7	0.86
1.5	31.6	2.5	23.6	0.86

3.3. Effects of urea concentration

Fig. 8A depicts Nyquist diagram for GC/NiO_x at different urea concentrations at E = 0.4 V (NiO_x loading time is 10 min). The range of urea concentrations is 0.05–1.5 M. The semicircle diameter decreases with the increase in the urea concentration before it slightly increases again at urea concentration [urea] > 0.5 M. An equivalent circuit similar to that shown in the inset of Fig. 4 is used to fit the data in Fig. 8A. Table 4 lists the fitting parameters of the given equivalent circuit that is used to fit the EIS results in Fig. 8A. As the concentration increases, the R_{ct} decreases up to a concentration of urea = 0.5 M before it slightly increases again (Fig. 8B). The decrease in R_{ct} may be

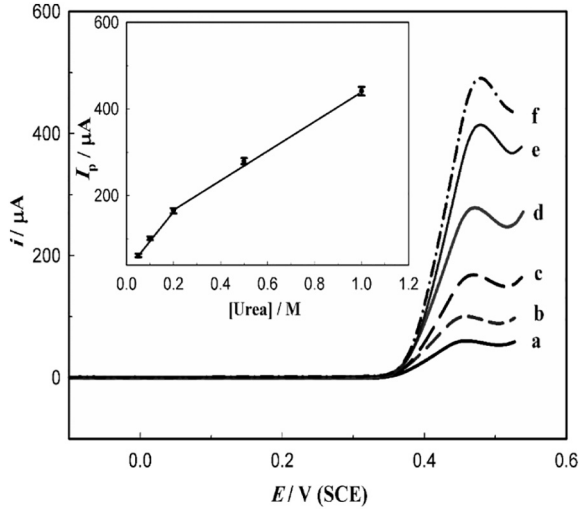

Fig. 9. LSVs for urea electrooxidation on GC/NiO_x at different urea concentrations at scan rate of 20 mV s^{-1}. The urea concentrations are: (a) 0.05, (b) 0.1, (c) 0.2, (d) 0.5 (e) 1.0 M and (f) 1.5 M. Inset shows the variation of the peak current with the [Urea].

attributed to the increase of the charge transfer kinetics (lower R_{ct}) due to higher rates of electrocatalytic oxidation of urea. The presence of higher concentrations of urea speed up the oxidation of Ni(II) to Ni(III) since Ni(III) is removed by urea and hence enhances further conversion of Ni(II) to Ni(III) and increases the rate of charge transfer (i.e., lower R_{ct}). The decrease in the rate of charge transfer kinetics (higher R_{ct}) at [urea] > 0.5 M may be attributed to the increase of the extent of poisoning of the GC/NiO_x surface with the intermediates and products of the urea oxidation process. Poisoning of anodes in direct methanol and direct formic acid fuel cells is well documented [48,49]. The main source of poisoning in the above fuel cells is the adsorbed CO molecules. In our case, urea oxidation, CO_2, NH_3 and CO_3^{2-} may be the main constituents of the poisoning products. According to Daramola [50], he suggested that the rate of urea oxidation was found to be highly dependent on desorption of carbon dioxide during the electrochemical oxidation process.

Fitting of the above data in Fig. 5B can be done using an equation developed by Danaee et al. [24]. The equation is given by;

$$R_{ct} = \frac{[k_1 + k_{-1} + 2k_2 C]^2}{[(2F^2 A\Gamma^* k_2 C k_1/RT)[2\alpha k_2 C + k_{-1}]} \quad (5)$$

where k_1, k_{-1} and k_2 are the rates constant of the equations shown in Eqs. (7), (8), C is the bulk concentration of urea, A is the electrode area, Γ^* is the total number of adsorption sites per unit area of the electrode surface and F, T and R have their regular meaning. Fig. 5B shows semiquantitative agreement between Eq. (5) and the data collected from impedance measurements. The values of the rates constant resulting from the fitting process were found to be; $k_1 = 1.4 \times 10^{-4}\ s^{-1}$, $k_{-1} = 80.1$ and $k_2 = 1.3 \times 10^{-3}\ cm^3\ mol^{-1}\ s^{-1}$.

3.4. Cyclic voltammetry performance

Discussion of the electrocatalytic oxidation of urea on the NiO_x modified electrode is introduced in this part. Fig. 9 depicts LSVs for urea electrooxidation on GC/NiO_x electrode at different urea concentrations at a scan rate of 20 mV s^{-1}. The inset shows the variation of the peak current, I_p with the urea concentrations ([urea]). The peak current increases with the urea concentration in a linear manner up to [urea] of 0.2 M. At [urea] > 0.2 M, the I_p increases but not with the same linear fashion. The above results suggest that urea oxidation is a diffusion-controlled process ([urea] < 0.2 M) at the present conditions.

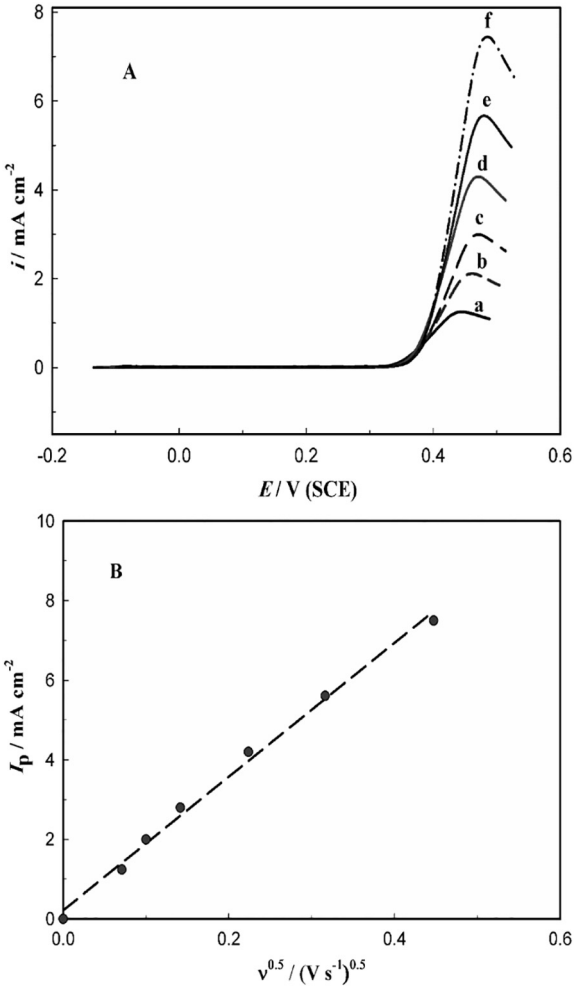

Fig. 10. A) LSV responses obtained at GC/NiO_x electrode in 0.5 M NaOH solution containing 0.2 M urea. Potential scan rate: (a) 5, (b) 10, (c) 20, (d) 50, (e) 100 and f) 200 mV s^{-1}. B) Relation of the I_p with the square root of the potential scan rate.

Fig. 10A depicts the LSVs responses of GC/NiO_x in 0.5 M NaOH containing 0.2 M urea at scan rates ranging from 5 to 200 mV s^{-1}. Note that the presented LSVs are all background-subtracted i.e., subtracted from the LSV at the same potential range but in the blank (0.5 M NaOH) i.e., urea-free electrolyte. The figure clearly demonstrates the increase of the peak current, I_p with the potential scan rate, ν with positive shift in the peak potential for the catalytic oxidation of urea. This is a characteristic of irreversible voltammetry behavior (see Fig. 6). Fig. 10B shows the linear relation of the peak current of urea oxidation with the square root of the potential scan rate, $\nu^{0.5}$. The dashed line represents the theoretical relation given by Randles–Sevcik equation and the symbols represent the experimental data (after subtraction from the background) . This indicates a typical behavior of mass transfer controlled reaction. The peak current, I_p of a diffusion-controlled totally irreversible process can be given by Randles–Sevcik equation (Eq. (6)) [51]:

$$I_p = 2.99 \times 10^5 n(\alpha n_a)^{0.5} A C D^{0.5} \nu^{0.5} \quad (6)$$

where I_p is the peak current, (A)n is the total number of electrons (n = 6), α is the charge transfer coefficient, n_a is the number of electrons in the rate determining step (n_a = 1), A is the surface area of the working electrode (cm^2), D is the diffusion coefficient of urea, C is the bulk concentration of urea(mole cm^{-3}) and v is the scan rate (V s^{-1}). The diffusion coefficient is calculated from the fitting of the theoretical plot based on Randles-Sevcik equation with the experimental data and it was found to be $D = 1.6 \times 10^{-6}\ cm^2\ s^{-1}$ using

$A = 0.07\ cm^2$ and $\alpha = 0.785$ [22]. This value of D is comparable with values reported in literature at similar conditions [21,22].

Based on the interesting electrochemical studies done by Botte [22,46], two possible mechanisms for the electrooxidation of urea molecules on a NiOOH catalyst in the alkaline medium were proposed. One is the direct oxidation and the other is indirect or catalyst regeneration (EC′) mechanism. In the direct oxidation mechanism urea is oxidized on the NiOOH electrode surface (Eqs. (1) and (2)). The indirect oxidation or catalyst regeneration (EC′) mechanism of urea on NiOOH catalyst is shown below [22,46].

At the anode:

$$\text{E } 6Ni(OH)_{2(s)} + 6OH^- \underset{k_{-1}}{\overset{k_1}{\longleftrightarrow}} 6NiOOH_{(s)} + 6H_2O_{(l)} + 6e^- \quad (7)$$

$$\text{C } 6NiOOH_{(s)} + CO(NH_2)_{2(aq)} + H_2O_{(l)} \overset{k_2}{\rightarrow} 6Ni(OH)_{2(s)} + N_{2(g)} + CO_{2(g)} \quad (8)$$

Net anodic reaction:

$$EC'CO(NH_2)_{2(aq)} + 6OH^- \rightarrow N_{2(g)} + 5H_2O_{(l)} + CO_{2(g)} + 6e^- \quad (9)$$

Hence, $Ni(OH)_2$ is anodically converted to NiOOH and consequently, the catalytically active NiOOH is chemically reduced to the inactive $Ni(OH)_2$ as a result of urea oxidation. Meanwhile, urea is chemically oxidized to products. The inactive $Ni(OH)_2$ will be electrochemically oxidized to NiOOH due to the prevailing high oxidation potential thus regenerating the catalyst for further oxidation of urea molecules. This is in accordance with the results shown in Fig. 6.

The discussion of Fig. 3 implies the reversibility of the NiOOH/Ni$(OH)_2$ wave in the 0.5 M NaOH solution. Also, from Fig. 6, in presence of urea in 0.5 NaOH, the regeneration of the $Ni(OH)_2$ catalyst will lead to the loss of reversibility of the NiOOH/$Ni(OH)_2$ wave and hence the anodic current density increases drastically. Thus;

$$Ni(OH)_{2(s)} + OH^- \rightleftarrows NiOOH_{(s)} + H_2O_{(l)} + e^- \quad (10)$$

$$NiOOH_{(s)} + urea_{(aq)} \rightarrow Ni(OH)_{2(s)} + \text{products} \quad (11)$$

The above two equations imply the catalyst regeneration as per the indirect oxidation of urea.

The activity of the used electrode here (GC/NiO_x) is found to be superior to similar catalysts (NiO) synthesized using electrochemical routes. For instance, the specific activity (in $mA\ cm^{-2}\ mg^{-1}$) in the present work is 177 $mA\ cm^{-2}\ mg^{-1}$. At similar conditions, this value was found to be 70.0 in Ref. [37], 21.0 in Ref. [22], 61.5 in Ref. [35] and 89.0 $mA\ cm^{-2}\ mg^{-1}$in Ref. [36]. Note that in the above references the NiO were synthesized in bulk scale rather than nanoscale. Clearly, using nanosize of the NiO_x in this work has more advantage than bulky sized catalysts. However, our value of specific activity was found to be less than others [38] and closer to others [52]. This may be attributed to the fact the latter references used nanosize NiO along with nanosize substrates such as nano graphene oxide [52]. The effects of the nanosized substrate need further study in order to fully understand this important electrochemical process.

4. Conclusions

NiO_x nanoparticles modified GC electrode showed enhancement of urea oxidation from an alkaline medium. Different techniques such as EIS and CV were used for studying the electrochemical characteristics of urea oxidation. The EIS study showed different shapes and values of the EIS fitting parameters depending on the loading extent of NiO_x and urea concentration. Optimization of the NiO_x loading and explanation of the effects of the NiO_x loading and urea concentration are enabled using the EIS and equivalent circuit parameters. Electrocatalytic oxidation of urea is consistent with Randles-Sevcik equation for a completely irreversible diffusion-controlled process.

References

[1] D.R. McCubbin, B.J. Apelberg, S. Roe, J.F. Divita, Livestock ammonia management and particulate-related health benefits, Environ. Sci. Technol. 36 (2002) 1141–1146.
[2] L. Zhou, Y.F. Cheng, Catalytic electrolysis of ammonia on platinum in alkaline solution for hydrogen generation, Int. J. Hydrog. Energy 33 (2008) 5897–5904.
[3] L. Rong, T. Shanwen, T. John, S. Irvine, A direct urea fuel cell—power from fertilizer and waste, Energy Environ. Sci. 3 (2010) 438–441.
[4] B. Sørensen, Hydrogen and Fuel Cells-emerging Technologies and Applications, 217 Elsevier Academic Press, 2005.
[5] L. Rong, T. Shanwen, Preparation of nano-sized nickel as anode catalyst for direct urea and urine fuel cells, J. Power Sources 196 (2011) 5021–5026.
[6] H.J. Bradley, Electrolytic destruction of urea in dilute chloride solution using DSA electrodes in a recycled batch cell, Water Res. 39 (2005) 2245–2252.
[7] C.C. Jara, S.D. Giulio, D. Fino, P. Spinelli, Combined direct and indirect electro-xidation of urea containing water, J. Appl. Electrochem. 38 (2008) 915–922.
[8] H.Q. Yu, Z.H. Zhu, W.R. Hu, H.S. Zhang, Hydrogen production from rice winery wastewater in an upflow anaerobic reactor by using mixed anaerobic cultures, Int. J. Hydrog. Energy 27 (2002) 1359–1365.
[9] W. Simka, J. Piotrowski, A. Robak, G. Nawrat, Electrochemical treatment of aqueous solutions containing urea, J. Appl. Electrochem. 39 (2009) 1137–1143.
[10] M.H. Cataldo, N. Russo, M. Panizza, P. Spinelli, D. Finoa, Electrochemical oxidation of urea in aqueous solutions using a boron-doped thin-film diamond electrode, Diam. Relat. Mater. 44 (2014) 109–116.
[11] D. Das, T.N. Veziroglu, Hydrogen production by biological processes: a survey of literature, Int. J. Hydrog. Energy 26 (2001) 13–28.
[12] F. Vitse, M. Cooper, G.G. Botte, On the use of ammonia electrolysis for hydrogen production, J. Power Sources 142 (2005) 18–26.
[13] Y. Liang, Q. Liu, A.M. Asiri, X. Sun, Enhanced electrooxidation of urea using $NiMoO_4xH_2O$ nanosheet arrays on Ni foam as anode, Electrochim. Acta 153 (2015) 456–460.
[14] J. Ren-Yu, C. Der-Sheng, J. J-Jiang, W. Mao-Sung, Formation of open-ended nickel hydroxide nanotubes on three-dimensional nickel framework for enhanced urea electrolysis, Electrochem. Commun. 29 (2013) 21–24.
[15] R.L. King, G.G. Botte, Hydrogen production via urea electrolysis using a gel electrolyte, J. Power Sources 196 (2011) 2773–2778.
[16] A.P.S. Terblanche, Health hazards of nitrate in drinking water, Water SA 17 (1991) 77–82.
[17] J.Y. Jiang, M. Chang, P. Pan, Simultaneous hydrogen production and electrochemical oxidation of organics using boron-doped diamond electrodes, Environ. Sci. Technol. 42 (2008) 3059–3063.
[18] I. Danaee, M. Jafarian, F. Forouzandeh, F. Gobal, M.G. Mahjani, Electrochemical impedance studies of methanol oxidation on GC/Ni and GC/NiCu electrode, Int. J. Hydrog. Energy 34 (2009) 859–869.
[19] M. Vidotti, M.R. Silva, R.P. Salvador, S.I.C. de Torresi, L.H. Dall, Antonia Electrocatalytic oxidation of urea by nanostructured nickel/cobalt hydroxide electrodes, Electrochim. Acta 53 (2008) 4030–4034.
[20] W. Zhang, S. Yin, X. Li, G. Xu, T. Xie, Impact of the alkali cation on the electrocatalytic oxidation of urea andbenzyl alcohol on nickel electrode, Electrochem. Commun. 63 (2016) 1–4.
[21] N.A.M. Barakat, M.H. El-Newehy, A.S. Yasin, Z.K. Ghouri, S.S. Al-Deyab, Ni & Mn nanoparticles-decorated carbon nanofibers as effective electrocatalyst for urea oxidation, Appl. Catal. A Gen. 510 (2016) 180–188.
[22] W. Yan, D. Wang, G.G. Botte, Electrochemical decomposition of urea with Ni-based catalysts, Appl. Catal. B Environ. 127 (2012) 221–226.
[23] B.K. Boggs, R.L. King, G.G. Botte, Urea electrolysis: direct hydrogen production from urine, Chem. Commun. 32 (2009) 4859–4861.
[24] I. Danaeea, M. Jafarian, A. Mirzapoora, F. Gobal, M.G. Mahjani, Electrooxidation of methanol on NiMn alloy modified graphite electrode, Electrochim. Acta 55 (2010) 2093–2100.
[25] I. Danaee, M. Jafarian, F. Forouzandeh, F. Gobal, M.G. Mahjani, Impedance spectroscopy analysis of glucose electro-oxidation on Ni-modified glassy carbon electrode, Electrochim. Acta 53 (2008) 6602–6609.
[26] N.S. Nguyen, D. Gautam, H.H. Yoon, Nickel/cobalt oxide-decorated 3D graphene nanocomposite electrode for enhanced electrochemical detection of urea, Biosens. Bioelectron. 77 (2016) 372–377.
[27] S. Prakash, T. Chakrabarty, A.K. Singh, V.K. Shahi, Polymer thin films sembedded with metal nanoparticles for electrochemical biosensors applications, Biosens. Bioelectron. 41 (2013) 43–53.
[28] Mao-Sung Wu, Guan-Wei Lin, Run-Song Yang, Hydrothermal growth of vertically-aligned ordered mesoporous nickel oxide nanosheets on three-dimensional nickel framework for electrocatalytic oxidation of urea in alkaline medium, J. Power Sources 272 (2014) 711–718.
[29] Dan Wang, Wei Yan, Santosh H. Vijapur, Gerardine G. Botte, Enhanced electro-catalytic oxidation of urea based on nickel hydroxide nanoribbons, J. Power Sources 217 (2012) 498–502.
[30] R. Ding, Li Qi, M. Jia, H. Wang, Facile synthesis of mesoporous spinel $NiCo_2O_4$ nanostructures as highly efficient electrocatalysts for urea electro-oxidation, Nano 6 (2014) 1369–1376.
[31] L. Wang, T. Du, J. Cheng, X. Xie, B. Yang, M. Li, Enhanced activity of urea electrooxidation on nickel catalysts supported on tungsten carbides/carbon nano-tubes, J. Power Sources 280 (2015) 550–554.
[32] N.A.M. Barakat, M. Motlak, Z.K. Ghouri, A.S. Yasina, M.H. El-Newehyd, S.S. Al-Deyab, Nickel nanoparticles-decorated graphene as highly effective and stable

electrocatalyst for urea electrooxidation, J. Mol. Catal. A Chem. 421 (2016) 83–91.
[33] F. Guo, Ke Ye, M. Du, X. Huang, K. Cheng, G. Wang, D. Cao, Electrochemical impedance analysis of urea electro-oxidation mechanism on nickel catalyst in alkaline medium, Electrochim. Acta 210 (2016) 474–482.
[34] J. Vilana, E. Gómez, E. Vallés, Influence of the composition and crystalline phase of electrodeposited CoNi films in the preparation of CoNi oxidized surfaces as electrodes for urea electro-oxidation, Appl. Surf. Sci. 360 (2016) 816–825.
[35] W. Yan, D. Wang, L.A. Diaz, G.G. Botte, Nickel nanowires as effective catalysts for urea electro-oxidation, Electrochim. Acta 134 (2014) 266–271.
[36] V. Vedharathinam, G.G. Botte, Understanding the electro-catalytic oxidation mechanism of urea on nickel electrodes in alkaline medium, Electrochim. Acta 81 (2012) 292–300.
[37] Mao-Sung Wu, Ren-Yu Ji, Yo-Ru Zheng, Nickel hydroxide electrode with a monolayer of nanocup arrays as an effective electrocatalyst for enhanced electrolysis of urea, Electrochim. Acta 144 (2014) 194–199.
[38] F. Guo, K. Ye, K. Cheng, G. Wang, D. Cao, Preparation of nickel nanowire arrays electrode for urea electrooxidation in alkaline medium, J. Power Sources 278 (2015) 562–568.
[39] S.M. El-Refaei, M.M. Saleh, M.I. Awad, Enhanced glucose electrooxidation at a binary catalyst of manganese and nickel oxides modified glassy carbon electrode, J. Power Sources 223 (2013) 125–128.
[40] S.M. El-Refaei, M.I. Awad, B.E. El-Anadouli, M.M. Saleh, Electrocatalytic glucose oxidation at binary catalyst of nickel and manganese oxides nanoparticles modified glassy carbon electrode: optimization of the loading level and order of deposition, Electrochim. Acta 92 (2013) 460–467.
[41] K.E. Toghill, L. Xiao, A. Michael, M.A. Phillips, G. Richard, R.G. Compton, The non-enzymatic determination of glucose using an electrolytically fabricated nickel microparticle modified boron-doped diamond electrode or nickel foil electrode, Sensors Actuators B 147 (2010) 642–652.
[42] H. Bode, K. Dehmelt, J. Witte, Nickel hydroxide electrodes, I. Nickel(II) hydroxide hydrate, Electrochim. Acta 11 (1966) 1079–1087.
[43] A.S. Adekunle, K.I. Ozoemena, Electron transfer behaviour of single-walled carbon nanotubes electro-decorated with nickel and nickel oxide layers, Electrochim. Acta 53 (2008) 5774–5782.
[44] A. Czerwinski, M. Dmochowska, M. Grden, M. Kopczyk, G.G. Wojcik, et al., Electrochemical behavior of nickel deposited on reticulated vitreous carbon, J. Power Sources 77 (1999) 28–33.
[45] A. Salimi, M. Roushani, S. Soltanian, R. Hallaj, Picomolar detection of insulin at renewable nickel powder-doped carbon composite electrode, Anal. Chem. 79 (2007) 7431–7438.
[46] V. Vedharathinam, G.G. Botte, Direct evidence of the mechanism for the electro-oxidation of urea on $Ni(OH)_2$ catalyst in alkaline medium, Electrochim. Acta 108 (2013) 660–665.
[47] D. Cibrev, M. Jankulovska, T. Lana-Villarreal, R. Go'mez, Oxygen evolution at ultrathin nanostructured $Ni(OH)_2$ layers deposited on conducting glass, Int. J. Hydrog. Energy 38 (2013) 2746–2753.
[48] C. Rice, S. Ha, R.I. Masel, P. Waszczuk, A. Wieckowski, T. Barnard, Direct formic acid fuel cells, J. Power Sources 111 (2002) 83–89.
[49] R.H. Tammam, M.M. Saleh, Electrocatalytic oxidation of formic acid on nano/micro fibers of poly (*p*-anisdine) modified platinum electrode, J. Power Sources 246 (2014) 178–183.
[50] D.A. Daramola, D. Singh, G.G. Botte, Dissociation rates of urea in the presence of NiOOH catalyst: a DFT analysis, J. Phys. Chem. A 114 (2010) 11513–11521.
[51] A.J. Bard, L.R. Faulkner, Electrochemical Methods: Fundamentals and Applications, second ed., Wiley, New York, 1980.
[52] D. Wang, W. Yan, S.H. Vijapur, G.G. Botte, Electrochemically reduced graphene oxide–nickel nanocomposites for urea electrolysis, Electrochim. Acta 89 (2013) 732–736.